Electron impact double ionization of neon, argon and molecular nitrogen: role of the two-step mechanism

C Li, A Lahmam-Bennani, E M Staicu Casagrande, C Dal Cappello

Electron impact double ionisation of neon, argon and molecular nitrogen: role of the two-step mechanism

C Li[1,2], A Lahmam-Bennani[1,2,§], E M Staicu Casagrande[1,2] and C Dal Cappello[3]

[1] Université Paris-Sud 11, Institut des Sciences Moléculaires d'Orsay (ISMO, UMR 8214), Bât. 351, 91405 Orsay Cedex, France
[2] CNRS-ISMO, Bât. 351, 91405 Orsay Cedex, France
[3] Université Paul Verlaine-Metz, Laboratoire de Physique Moléculaire et des Collisions, ICPMB (FR 2843), Institut de Physique, 1 rue Arago, 57078 Metz Cedex 3, France

[§] author to whom all correspondence should be addressed
e-mail : azzedine.bennani@u-psud.fr

PACS 34.80.Dp (also 34.50.Fa and 34.80.-I, and 34.10.+x)

Abstract

Recent measurements of the (e,3-1e) four-fold differential cross sections (4DCS) for double ionisation of helium are here extended to more complex targets, namely neon, argon and molecular nitrogen. The previous observations of large angular shifts in the experimental 4DCS distributions with respect to the momentum transfer axis and the existence of structures in these distributions are found to similarly hold here. For the three investigated targets, the experimental data are compared with the kinematical analysis previously given to describe the second order, ‘two-step 2’ double ionisation mechanism. Such comparison confirms our interpretation which allows relating the observed shifts and structures in the intensity distributions mostly to the ‘two-step 2’ mechanism, which is shown to predominate over the first-order ‘shake-off’ and ‘two-step 1’ mechanisms under the present kinematics. The experimental data are also compared to the predictions of a first Born and a second Born model, showing a rather mixed agreement.

1. Introduction

In two recently published papers [1,2] Lahmam-Bennani and coworkers reported four-fold differential cross sections (4DCS) measurements for electron impact double ionisation (DI) of helium atom at an impact energy in the range E_0 ~ 600 – 700 eV and for a large sampling of ejected electron energies. The main experimental finding in these works was that the experimental angular distributions of the 4DCS displayed large angular shifts of the forward and backward lobes with respect to the momentum transfer direction or it's opposite, respectively, as well as a breaking of symmetry with respect to these directions. A kinematical interpretation was given in [1] which allows relating the observed shifts and the existence of structures in the intensity distributions mostly to the second order, 'two-step 2' (TS2) DI mechanism, which was shown to predominate over the first-order 'shake-off' (SO) and 'two-step 1' (TS1) mechanisms under the considered kinematics. (For a discussion of the various DI mechanisms, see for instance [3-7]). This kinematical interpretation was nicely confirmed in [2] by the results of two model calculations which include non-first order mechanisms. The first model named TS2-MCEG is based on the first Born approximation (FBA), but where higher order effects are incorporated using the Monte Carlo Event Generator (MCEG) technique [8] to simulate the TS2 mechanism by convoluting two single ionisation (SI) events which are both calculated in the FBA. These are successively the SI of the He atom by the incident electron and that of the resulting He^+ ion by the intermediate scattered electron. The second theoretical model is more elaborate as it makes use of the second Born (B2) approximation and the closure approximation in the way described in [9]. Both these models were found to very clearly constitute a considerable improvement with respect to a first Born prediction as they succeeded in reproducing both the positions and the main structures of the forward and backward lobes.

The aim of the present work is to extend the work in [1,2] to other targets than helium (we use here two atomic targets, neon and argon, and one small molecule, molecular nitrogen N_2), in order to validate or invalidate the observations and the kinematical analysis therein given. Indeed, this analysis is merely dependent on the target species used. For given scattered and ejected electron energies, the target dependence does only enter *via* the small change in incident energy (< ~4%) due to the differences in the targets SI and DI potentials. Our objective is to add further experimental evidence that at the impact energy of the present work (~ 600-700 eV), DI of small atoms or molecules is dominated by non-first order mechanisms such as TS2, similar to the Helium case. This gives a kind of "universal", target

independent character to the observed shifts and positions of the 4DCS forward and backward lobes.

The present experimental data for Ne and Ar will be compared to first order theoretical results as well as to non-first order, second Born calculations where available. Due to the complex nature of the molecular target N_2, no elaborate calculations are available at the time of writing.

2. Experiment

The experimental set-up and procedure used in the present work are identical to those used in [1,2] and are described in detail in [10]. Briefly, a well-collimated electron beam with energy E_0 ~ 600 – 700 eV (see below) ionises a gas jet formed at the collision centre by the effusive flow of gas through a small capillary. Three high-efficiency, multi angle toroidal electrostatic energy analysers coupled to three position sensitive detectors allow observation of the final state electrons in the collision plane defined by the incident and scattered momentum vectors, $\boldsymbol{k_0}$ and $\boldsymbol{k_a}$, respectively. The fast, forward-scattered electron (indexed 'a') is detected at the scattered energy E_a = 500 eV and at two symmetrical scattering angles, θ_a = + (6°± 3°) and – (6°± 3°) as set by input slits at the entrance to the 'a'-toroidal analyser. Throughout this work, positive angles are counted clockwise starting from the incident electron beam direction. Among the two ejected electrons resulting from DI of the target, (labelled 'b' for the faster and 'c' for the slower), we choose to only detect the faster one, with energy E_b, in coincidence with the 'a'-scattered electron, hence a so-called (e,3-1e) experiment. Of course, such distinction does not hold for the case of equal ejection energies, but the same labelling 'b' is kept for the detected electron. These 'b'-electrons are multi-angle analysed in a double toroidal analyser over the angular ranges θ_b = 20° – 160° and 200° – 340°, where 0° is defined by the incident beam direction. In the off-line analysis, the total θ_b-angular range is divided into sectors of width $\Delta\theta_b$ = 5°. Though the emission direction of the third, 'c'-electron is unknown, its kinetic energy E_c is known from the energy conservation $E_0 - IP^{2+} = E_a+E_b+E_c$, where IP^{2+} is the target first DI potential leaving the ion in its ground state. (Here, it is assumed, following van der Wiel and Wiebes [11] that the DI process removing two electrons from the outermost orbital with the ion left in its ground state largely dominates DI processes with excited ion states). For each of the three considered targets (Ne, Ar and N_2), the experiments were performed at three ejected electron energies for the 'b'-electron, E_b = 12, 72 and 144 eV and a fixed 'c'-electron energy, E_c = 12 eV, hence

corresponding either to an equal or an unequal energy sharing (E_b:E_c) among electrons 'b' and 'c'. We also note the very large range of energy loss (E_0 - E_a) suffered by the projectile, from 67 to ~ 219 eV. The incident energy (E_0) is consequently adjusted to fulfil the energy conservation requirement for the target under study, with IP^{2+} = 62.6, 43.2 and 43.0 eV for Ne, Ar and N_2, respectively. The investigated kinematical conditions are listed in Table 1.

	E_a = 500 eV		θ_a = - 6 deg	E_c (undetected) = 12 eV
Target	E_0 **(eV)**	E_b **(eV)** detected	θ_K / θ_{-K} (deg)	$\theta_{F\text{-}TS2}$ / $\theta_{B\text{-}TS2}$ (deg)
	718.6	144	27 / 207	67 / 315
Ne	646.6	72	36 / 216	77 / 299
	586.6	12	50 / 230	86 / 280
	699.2	144	29 / 209	67 / 318
Ar	627.2	72	40 / 220	77 / 301
	567.2	12	56 / 236	87 / 278
	699	144	29 / 209	67 / 318
N_2	627	72	40 / 220	77 / 301
	567	12	56 / 236	87 / 278

Table 1. Kinematical parameters considered in this study. The last column indicates the forward and backward directions of ejection of the 'b'-electron ($\theta_{F\text{-}TS2}$ and $\theta_{B\text{-}TS2}$, respectively) as predicted by our kinematical model, see text.

Given the above experimental parameters, the momentum transfer to the target, defined by $\boldsymbol{K} = \boldsymbol{k_0} - \boldsymbol{k_a}$, varies in the magnitude from K = 0.76 au at E_0 = 567 eV to K = 1.39 au at E_0 = 718.6 eV, while its direction θ_K (shown in the 4th column of Table 1) varies from ~ 56° to ~ 27° for these two extreme cases. Simultaneously, due to the ±3° acceptance in θ_a -angle, the momentum transfer resolution amounts to ΔK ~ ± 0.2 au and the spread in the momentum transfer direction is $\Delta\theta_K$ ~ ±10°.

3. Results and discussion

The angular distributions of the (e,3-1e) four-fold differential cross sections (4DCS), $d^4\sigma/dE_a dE_b d\Omega_a d\Omega_b$, for DI of the outermost orbitals of Ne ($2p^{-2}$), Ar ($3p^{-2}$) and N_2 $(3\sigma_g)^{-2}$ are shown in figures 1 to 3, respectively at the three energy sharings (E_b:E_c) listed in Table 1. As a general observation, we find for all targets and all energy cases about the same behavior as

for He, i.e. all angular distributions display a forward and a backward lobe. Here, the labels forward lobe and backward lobe designate the lobe pointing roughly in the momentum transfer direction (+***K***) and in the opposite direction (-***K***), respectively. These two directions are indicated by the vertical dotted lines in the figures. We also observe that both lobes are not symmetrically distributed about ±***K*** axis and that their maxima are shifted from this axis direction by large amounts, ~30° to 60°. The uncertainty of ~10° in the momentum transfer direction is significantly smaller than the observed shift, and hence it only marginally affects this shift. Also, these lobes exhibit more or less pronounced structures.

To better understand the origin of these features, the experimental data are compared with the calculated results obtained for Ne using the first Born - three Coulomb waves (B1-3C) model. In this model, the initial state is described by a Hartree-Fock wave function of Clementi and Roetti [12]. The final state is described by the product of three Coulomb waves [13,14]. Two of these Coulomb functions describe each electron in the field of the target nucleus and the third function describes one electron in the field of the second electron, i.e. electron-electron correlation. Still for Ne, this B1-3C model was simplified by replacing the third Coulomb function by the Gamow factor, hence the name B1-2CG [15]. The B1-2CG results differed from those of the B1-3C model only in magnitude, the shape of the angular distributions being essentially unchanged. Consequently, due to the very long computational time needed for the full B1-3C model, it was decided to perform only B1-2CG calculations for the Ar case. For both Ne and Ar targets, we have included the contributions of the three residual states, namely ^{3}P, ^{1}D and ^{1}S. Both these B1 calculations are shown as dashed curves (B1-3C) and dotted curves (B1-2CG) in Fig. 1 and 2, where available. We recall here that they only include first-order DI mechanisms, namely the SO and TS1. To account for the second-order TS2 mechanism, calculations were also performed for Ne and Ar within the framework of the second Born approximation where the final state is described by the approximate 2CG wave function (two Coulomb functions plus Gamow factor, hence the name B2-2CG for this model). Here again, the use of the full 3C wave function with the second Born approximation needs much computer time especially for (e,3-1e). The B2-2CG results are shown as full curves in Fig. 1 and 2. For N_2 molecule, no similar B1 nor B2 theoretical results do exist. Note that the experiments are obtained on a relative scale and are normalized to the calculations at the maximum of the forward lobe.

A strong disagreement is found between first Born calculations and experiments for Ne and Ar, the disagreement being appreciably more pronounced than was observed previously for He [1,2]. Indeed, for both atomic targets the B1-3C and B1-2CG models yield forward and

backward angular distributions which are symmetrically distributed about $\pm\boldsymbol{K}$ directions, as it is expected from any first-order theory, whereas the experiments do not show such symmetry. Also, for the equal energy sharing case (Fig. 1(a) and 2(a)) the theoretical results display a marked minimum in the $\pm\boldsymbol{K}$ directions which is not observed in the experiments. Moreover, the theory predicts a rather small backward intensity (relative to the forward one), smaller than the experimental findings. These observed deviations between experimental data and first order theory are clear evidence that strong non-first Born effects are present in the (e,3-1e) 4DCS distributions, that is, the contribution of the TS2 or higher order mechanisms to the DI process is sufficiently important with respect to that of SO and/or TS1 to impose its finger print on the angular distributions. We thus so confirm the observations made for He in [1,2] and earlier in [16]. However, the qualitative success of the second Born B2-2CG model reported for He is far from being found again here in the Ne and Ar cases. Indeed, when compared to B1-2CG predictions, the B2-2CG model does yield a breaking of symmetry with respect to $\pm\boldsymbol{K}$ directions (at least in the case of Fig. 1(a) and 2(a)) as seen in the experiments. But, if one excludes the difference in magnitude of the cross section (not relevant here), the small change in the shape of the angular distributions is not sufficient to bring the B2-2CG results in significantly better agreement with experiments than B1-2CG. The disagreement between our B2-2CG model and experiments here is certainly due to the approximations made for treating double ionisation of a noble gas. In this case we reduce the problem of a 6-electron target (np^6) to that of two active electrons (the two ejected electrons) [17]. Moreover, Dal Cappello *et al* [9] have shown that the closure approximation used in B2 model yields results which strongly depend on the value of the parameter $\overline{w}$ used, where $\overline{w}$ is the average excitation energy. We notice that we used here the same parameter value for the cases of the double ionisation of noble gases as for helium.

We now aim to apply to our new results the kinematical analysis proposed in [1] and which has proven highly successful for the He case. This analysis is meant to give a qualitative interpretation of the observed structures as well as an estimate of the angular positions of the lobes in terms of physical effects included in the TS2 mechanism. The full details of this analysis have been previously reported in [1] and so are only briefly summarized here. TS2 is a two-step process, which is assumed to proceed via two successive (e,2e) ionisations of the target: in the first step, the 'c'-electron is ejected while the projectile is scattered with the highest probability at the $\pm\theta_{a*}$ angle corresponding to the Bethe ridge [18,19]. This intermediate 'a*'-scattered electron acts as a new projectile in a second (e,2e)

ionisation of the intermediate, singly charged ion, resulting in the pair ('a':'b') of electrons effectively detected. These are the 'a'-scattered one, observed with E_a = 500 eV under θ_a = -6°, and the 'b'-ejected one which appears mostly along the corresponding momentum transfer direction of this new collision, either in the forward direction or in the backward direction, noted $\theta_{F\text{-}TS2}$ and $\theta_{B\text{-}TS2}$, respectively, depending whether the intermediate 'a*'-electron is scattered under $+\theta_{a*}$ or $-\theta_{a*}$.

The so predicted $\theta_{F\text{-}TS2}$ and $\theta_{B\text{-}TS2}$ values are listed in the last column of Table 1 for each of the kinematics considered here. They are also indicated in Fig. 1-3 by the vertical dashed lines. We have already pin-pointed the fact that all the experimental data shown in Fig. 1-3 do display prominent structures for both the forward and the backward distributions, though may be less so for the molecular target, N_2. Remarkably, the predicted $\theta_{F\text{-}TS2}$ and $\theta_{B\text{-}TS2}$ values nicely agree with the angular positions of the structures located at the largest angles. This holds for all energy sharings considered in this work, from equal (panels (a)) to highly unequal (panels (c)) sharing. We thus conclude that the forward and backward structures positions in Fig. 1-3 are strongly influenced by the TS2 contribution, according to the above qualitative kinematical analysis where the TS2 process is considered as two successive, independent (e,2e) SI of the target. The first-order SO and TS1 contributions might of course be also present. Their contributions should be at their maximum in the momentum transfer direction, θ_K, and its opposite, θ_{-K}, but their intensity appears there to be appreciably smaller than that of the TS2, more so for the backward lobe.

It is worthwhile noting that the positions $\theta_{F\text{-}TS2}$ and $\theta_{B\text{-}TS2}$ predicted by our model are generated from purely kinematical considerations; hence they almost do not depend on the target for a given set of energies (E_a, E_b, E_c) and fixed scattering angle θ_a. The weak target dependence (see last column of Table 1 for a numerical illustration of this point) only shows up *via* the small change in incident energy (ΔE_0 < ~4%) due to the change in SI and DI potentials of the considered targets. The same statement holds for the positions θ_K and θ_{-K} which define the momentum transfer axis, and hence the position of the "first-order lobes". Therefore, within our kinematical model the shift $\Delta\theta_b$ of the predicted lobes from $\pm\boldsymbol{K}$ axis is quasi-independent of the target. Even more, it is also quasi-independent of the s or p character of the ionised orbital (we recall that we deal here with two electrons ejected from the 2p, 3p or $3\sigma_g$ orbital of Ne, Ar and N_2, respectively). This is indeed the experimental finding, where $\Delta\theta_b$ is practically constant in Fig. 1-3, for the same (E_b:E_c). This gives a kind of "universal", target

independent character to the observed shifts and positions of the 4DCS forward and backward lobes.

We may note from Fig. 1-3 that the measured forward and backward angular distributions exhibit more structures than the ones located at about $\theta_{F\text{-}TS2}$ and $\theta_{B\text{-}TS2}$ and which we interpret as being due to TS2 contribution, or those located at about θ_K and θ_{-K}, and which we attribute to SO and/or TS1 contributions. The origin of these additional structures may be diverse [2]. For instance, some of these structures may be due to other higher-order mechanisms not considered here within our kinematical model. A possible such candidate is the Two-Step1–Elastic mechanism (TS1-El) recently invoked by Schulz *et al* [20] in the context of fast p + He collisions. It can be viewed as follows: first, a TS1 process leads to the ejection of both target electrons, and then the projectile is elastically scattered from one of the two continuum electrons (hence the alternative label '3steps – 2 interactions' 3S2).

Also, we want to make two additional comments. First one is related to the ambiguity carried by the (e,3-1e) experiments, for these are not *fully* differential experiments due to the integration over the undetected 'c'-electron. For DI of He($1s^{-2}$), its kinetic energy E_c is known from the energy conservation $E_0 - IP^{2+} = E_a+E_b+E_c$, where IP^{2+} is the He DI potential. But for the more complex targets Ne, Ar and N_2, the final state of the ion is not determined, so that there is not just one single possible energy for the undetected 'c'-electron, but several discrete E_c values in the case of DI. (Triple or higher order ionisation would yield a whole continuum of energies E_c but the choice made here of E_c = 12 eV, that is E_c smaller than (IP^{3+} - IP^{2+}) does not allow triple or higher order ionisation to take place). A complete (e,3e) experiment is needed to resolve this ambiguity. Nevertheless, according to van der Wiel and Wiebes [11], the DI process removing two electrons from the outermost orbital with the ion left in its ground state should largely dominate higher order processes.

Our final comment is about the cross section distributions in Fig. 1-3. These two-lobes distributions look roughly like (e,2e) SI distributions, which are made of the familiar binary and recoil peaks. It is well established (see e.g. [21]) that, in the incident and ejected energy ranges considered here, the recoil-to-binary (R/B) maximum intensity ratio for the (e,2e) SI case is generally, although not systematically, smaller than unity and is rapidly decreasing with increasing ejected electron energy. In contrast, we observe here for the case of DI a backward-to-forward (B/F) maximum intensity ratio which is more or less constant *vs* E_b. [We note from Fig. 2 that DI of Ar($3p^{-2}$) is a special case in this respect, for it shows first a decrease then an increase of the B/F ratio when increasing E_b, similar to the peculiar behavior reported for the B/R ratio in the SI of Ar($3s^{-1}$) [21]]. This different behavior of the B/F and

B/R ratios in DI and SI, respectively, gives an additional proof (if at all necessary) of the very fundamental difference in nature between DI and SI. In particular, the recoil lobe in (e,2e) SI has a very different origin from that of the backward lobe in (e,3e) DI, the former being due to a backscattering of the ionised electron from the nucleus, whereas for the latter the intervention of the nucleus is not strictly needed as is the case for instance in our kinematical model.

4. Conclusion

The previous (e,3-1e) experiments for DI of helium at few hundred eV impact energy are here extended to more complex targets, namely neon, argon and molecular nitrogen. Compared to He, the ejected electron angular distributions exhibit similar features, that is large shifts from the momentum transfer axis as well as marked structures in the forward and backward lobes. For Ne and Ar, these features are not reproduced by a first Born B1-3C model, nor by a second Born (B2-2CG) model which does only slightly better. At the time of writing there exist neither elaborate first order nor second order calculations to which the present experimental data for N_2 could be compared. The kinematical description of the two-step 2 mechanism developed in [1] is applied to these new data, and it is shown to successfully predict the angular positions of some of the structures of the measured lobes. This work together with the previous one on He thus constitutes a large body of experimental evidence that under the present kinematics the TS2 mechanism dominates over first order SO and TS1 mechanisms. We also observe that the measured angular shifts of the forward and backward lobes are quasi- independent of the nature of the target, as also supported by our kinematical model.

Acknowledgment

C Li wishes to acknowledge a PhD grant from the China Scholarship Council.

Caption to figures

Figure 1 (Colour online): Relative four-fold differential cross sections (4DCS) for double ionisation of Ne ($2p^{-2}$). The scattered electron with energy E_a = 500 eV is detected at an angle θ_a = – 6° in coincidence with the fast-emitted electron with energy E_b, whereas the slow-emitted electron with energy E_c remains undetected. Panel (a): (E_b : E_c) = (12 : 12) eV, (b): (E_b : E_c) = (74 : 12) eV, (c) (E_b : E_c) = (144 : 12) eV. Full squares are the experimental data, with one standard deviation statistical error bar. Theoretical predictions from the first-Born B1-3C, B1-2CG and the second Born B2-2CG models are shown with the dashed green curve, the dotted black curve, and the full blue curve, respectively. The 4DCS scale shown is arbitrary, where experimental and theoretical results are inter-normalised for best visual fit at the maximum of the forward lobe. The thin dotted vertical lines indicate the direction of the momentum transfer (θ_K) and its opposite (θ_{-K}). The heavy dashed vertical lines indicate the directions of ejection of the 'b'-electron, ($\theta_{F\text{-}TS2}$ and $\theta_{B\text{-}TS2}$) as predicted by the given kinematical analysis, see text.

Figure 2 (Colour online): Same as in figure 1 but for double ionisation of Ar ($3p^{-2}$).

Figure 3 (Colour online): Same as in figure 1 but for double ionisation of N_2 $(3\sigma_g)^{-2}$.

References

[1] Lahmam-Bennani A, Staicu Casagrande E M, Naja A, Dal Cappello C and Bolognesi P 2010 *J. Phys. B: At. Mol. Opt. Phys.* **43** 105201

[2] Staicu Casagrande E M, Li C, Lahmam-Bennani A, Dal Cappello C, Schulz M and Ciappina M 2011 *J. Phys. B: At. Mol. Opt. Phys.* **44** 055201

[3] Carlson T A and Krause M O 1965 *Phys Rev* **140** 1057

[4] McGuire J H 1982 *Phys. Rev. Lett.* **49** 1153

[5] Tweed R J 1992 *Z. Phys. D.: At., Mol. Clusters* **23** 309

[6] El Marji B, Schröter C, Duguet A, Lahmam-Bennani A, Lecas M. and Spielberger L 1997 *J.Phys.B: At.Mol.Opt.Phys.* **30**, 3677

[7] Schröter C, El Marji B, Lahmam-Bennani A, Duguet A, Lecas M. and Spielberger L 1998 *J.Phys.B: At.Mol.Opt.Phys.* 31 131

[8] Ciappina M F, Schulz M and Kirchner T 2010 *Phys. Rev.* A **82** 062701

[9] Dal Cappello C, Haddadou A, Menas F and Roy A C 2011 *J. Phys. B: At. Mol. Opt. Phys.* **44** 015204

[10] Catoire F, Staicu Casagrande E M, Lahmam-Bennani A, Duguet A, Naja A, Ren X G, Lohmann B and Avaldi L 2007 *Rev. Sci. Instrum.* **78** 013108

[11] van der Wiel M J and Wiebes G 1971 *Physica* **53** 225

[12] Clementi E and Roetti C 1974 *At. Data Nucl. Data Tables* **14** 177

[13] Joulakian B, Dal Cappello C and Brauner M 1992 *J. Phys. B: At. Mol. Opt. Phys.* **25** 2863

[14] Ancarani L U, Gasaneo G, Colavecchia F D and Dal Cappello C 2008 *Phys. Rev.* A **77** 062712

[15] Hda H, Dal Cappello C and Langlois J 1994 *Z. Phys . D.* **29**, 25

[16] Lahmam-Bennani A, Duguet A and Roussin S 2002 *J. Phys. B: At. Mol. Opt. Phys.* **35** L59

[17] Dal Cappello C, Hda H and Roy A C 1995 *Phys. Rev. A.* **51**, 3735

[18] Lahmam-Bennani A, Wellenstein H F, Dal Cappello C, Duguet A and Rouault M 1983 *J. Phys. B* **16**, 2219

[19] Avaldi L, Camilloni R, Fainelli E, Stefani G, Franz A, Klar H and McCarthy I E 1987 *J. Phys. B: At. Mol. Phys.* **20** 5827

[20] Schulz M, Ciappina M F, Kirchner T, Fischer D, Moshammer R and Ullrich J 2009 *Phys. Rev.* A **79**, 042708

[21] Kheifets A S, Naja A, Staicu Casagrande E M and Lahmam-Bennani A 2009 *J. Phys. B: At. Mol. Opt. Phys.* **42** 165204

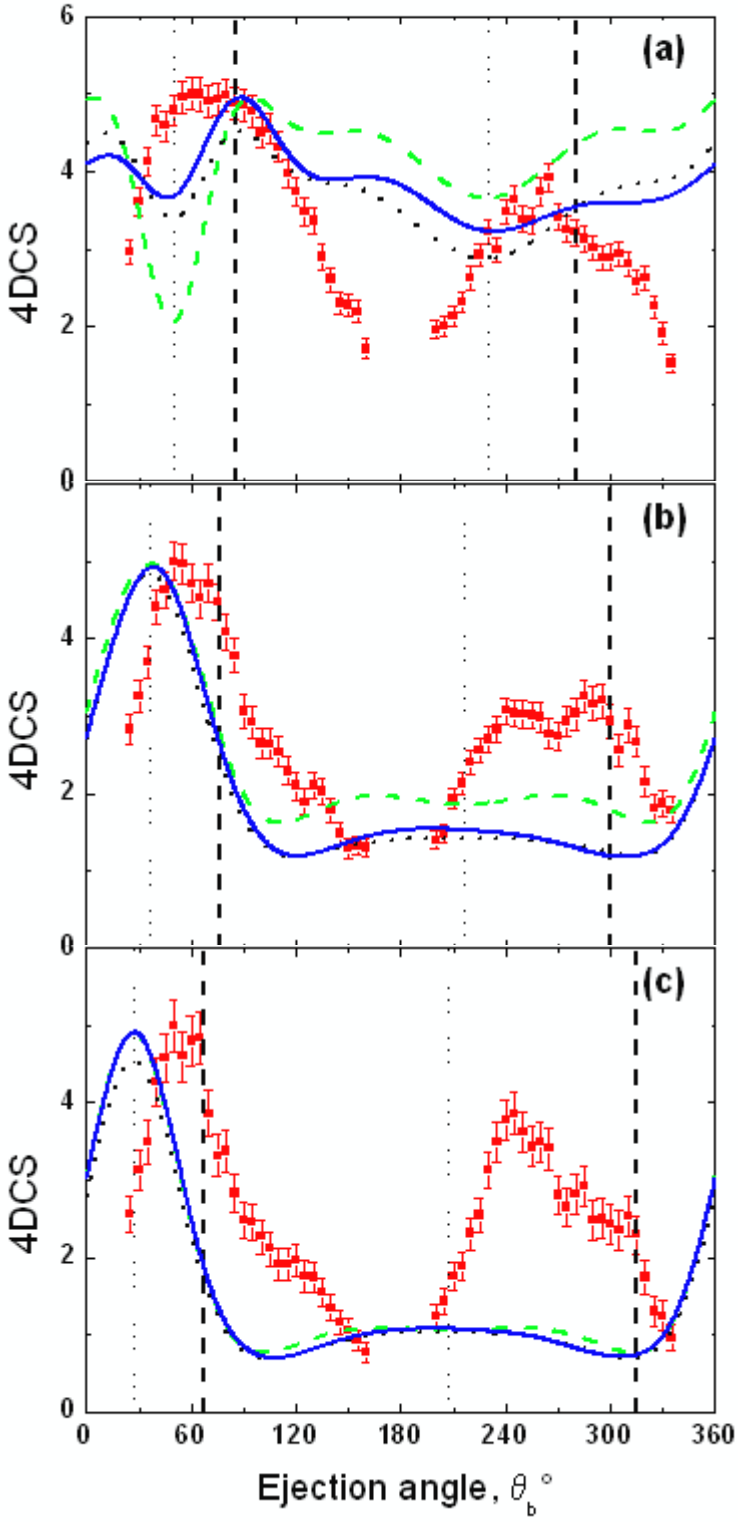

Fig 1 (Neon)
C Li *et al*

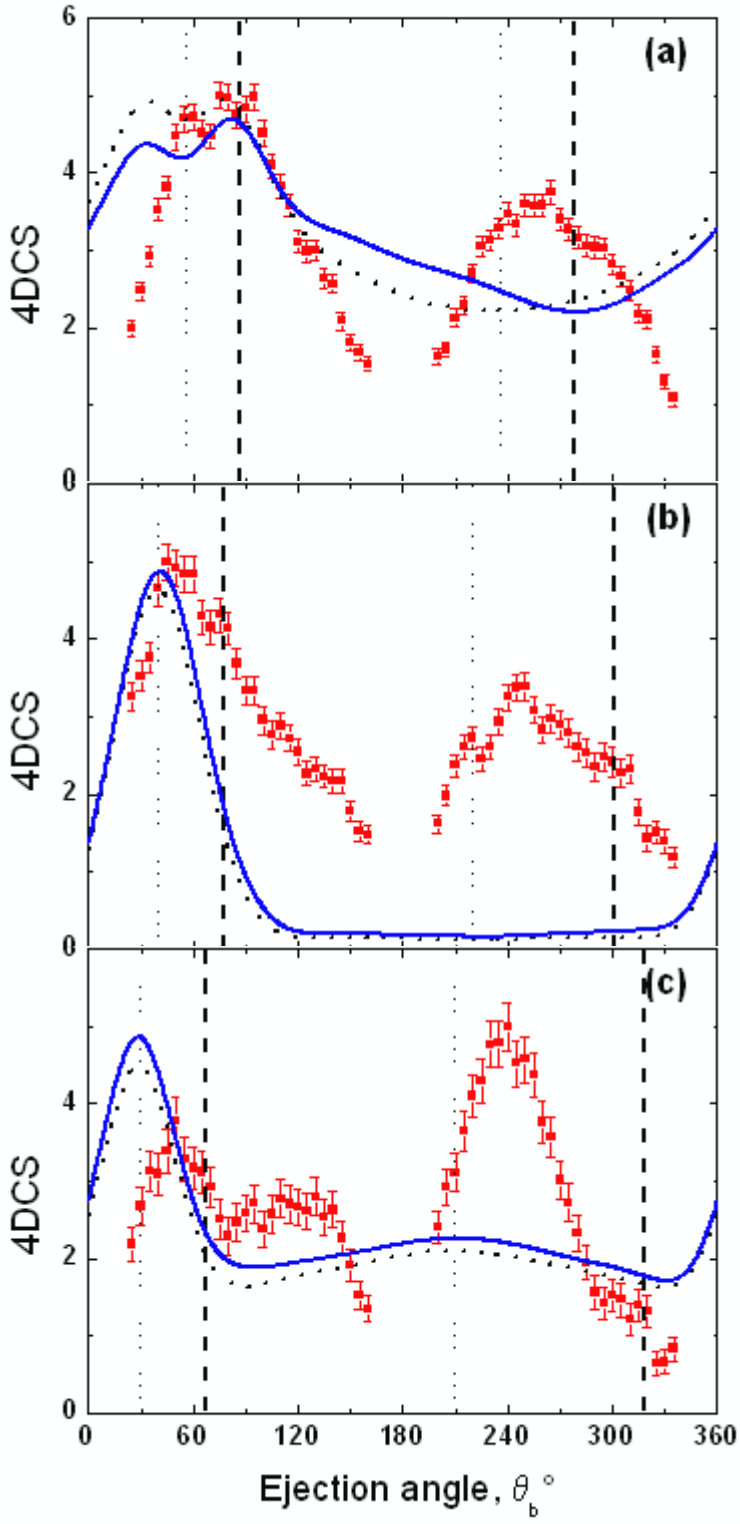

Fig 2 (Argon)
C Li *et al*

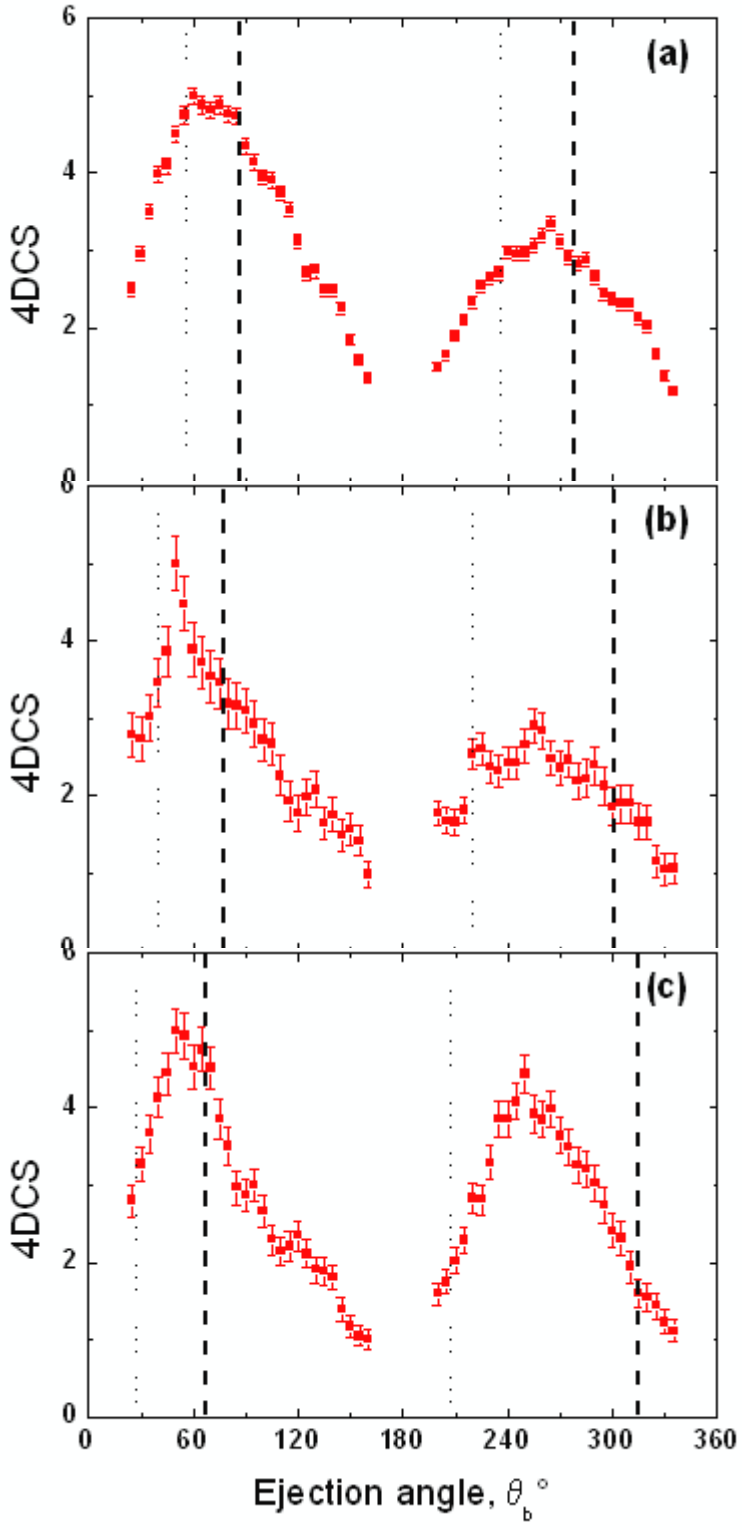

Fig 3 (Nitrogen)
C Li *et al*